3D structure of the non-linear ELM phase

RP Wenninger[1], H Reimerdes[2], O Sauter[2], H Zohm[3]

[1] *Universitätssternwarte der Ludwig-Maximilians-Universität, 81679 München, Germany*

[2] *Ecole Poytechnique Fédérale Lausanne (EPFL), CRPP, Euratom Association, Lausanne, Switzerland*

[3] *Max-Planck-Institut für Plasmaphysik, EURATOM Association, Garching, Germany*

Edge localised modes (ELMs) allow sufficient purity of tokamak plasmas to be maintained and thus enable stationary H-mode. However in a future device large unmitigated ELMs are believed to cause divertor power flux densities far in excess of tolerable material limits. Hence the size of energy loss per ELM and the resulting ELM frequency must be controlled. The ELM size is determined by its non-linear evolution [1, 2]. It is therefore important to understand the non-linear evolution of the ELM associated perturbation and the resulting pedestal erosion in 3D. This paper concentrates on an analysis of the toroidal structure of magnetic perturbations during type I ELMs in TCV.

The operational space of the TCV tokamak [3] includes H-mode plasmas in X-point configuration with a wide range of plasma shapes. Discharge 42062 is performed in a diverted lower single null configuration [4]. Key parameters are: Plasma current 300kA, magnetic field on magnetic axis 1.43T, safety factor at 95% poloidal flux 2.3, central (pedestal top) electron density $5\times10^{19}\mathrm{m}^{-3}(3.8\times10^{19}\mathrm{m}^{-3})$, central (pedestal top) electron temperature 2.5keV (0.5keV). The discharge is heated with 135kW ohmic power, 900kW ECRH power (X3) launched from the top of the vacuum vessel and 520kW ECRH power (X2) launched from the low field side in the X-point vicinity. In a similar discharge (42547) an increase in X2 input power leads to an increase in ELM frequency, documenting the type I character of these ELMs [4].
TCV is equipped with an extensive set of magnetic probes, which are mounted on the inner wall of the vacuum vessel [5]. All magnetic data presented in this paper are acquired by a set of 16 toroidally equally spaced probes in identical poloidal positions on the magnetic low field side (LFS). These probes sample the time derivative of the poloidal magnetic field component tangential to the wall with 250kHz.
The time, at which the D_α-radiation from divertor and main chamber exceeds 5% of its maximum value during the ELM, is used as ELM reference time $t_{D\alpha,ons}$.

The magnetic perturbation δB, which is the focus of this work, is obtained by integration from $t_{D\alpha,ons}-0.15$ms and subtraction of the $n=0$ component. Figure 1(a) shows the magnetic perturbation δB during an ELM in discharge 42062 as function of time t and toroidal angle ϕ. This type of data presentation allows to identify trajectories of peaks and dips of δB in $\phi-t-$space. A trajectory of a peak of δB obtained by application of a dedicated tracing algorithm is also illustrated in figure 1(a). Figure 1(b) displays the evolution of the perturbation on the trajectory (δB_{traj}) and D_α-radiation. Assuming the perturbation is field aligned during the growth phase of δB_{traj}, the propagation direction of single excursions can be mapped into the electron diamagnetic drift direction as observed earlier on other experiments [6–8].

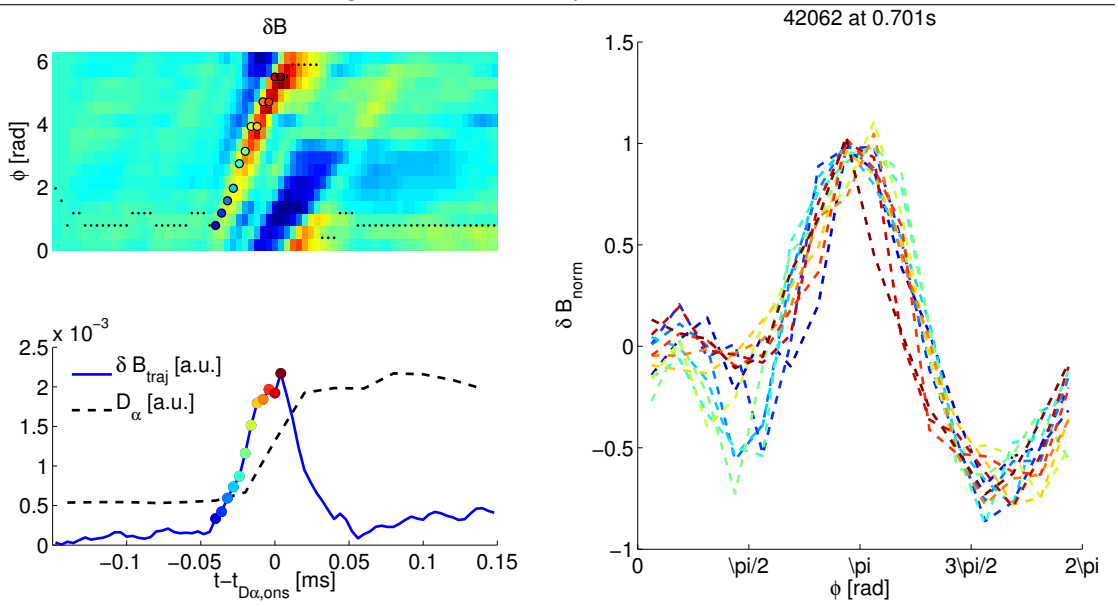

Figure 1: Evolution of profiles of δB in the rise phase of an ELM at 0.7011s in discharge 42062: (a) δB as function of t and ϕ. The identified trajectory is marked by dots (the larger ones in color indicate time steps shown in (c)). (b) Evolution of δB_{traj} and D_α-radiation during the same time interval. (c) Shifted toroidal profiles of δB normalized by δB_{traj}(t). For the identification of time instances the same color code as for the dots in (a) and (b) is used.

Figure 1(c) shows the evolution of toroidal profiles of δB for an ELM during a phase, in which δB_{traj} is growing more than a factor of 10 up to its maximum value. The profiles have been shifted for each time instance in a way, that the main peak is at a fixed toroidal position[1] and normalized by δB_{traj}. The minimum at $\phi \sim 1.5$ has some evolution in relative depth. However the fundamental shape of the profile is maintained throughout the entire time interval displayed and may be described as *stiff*. A similar behavior has been observed for the vast majority of ELMs.

This observation documents that the temporal and the spatial dependence of the magnetic perturbation are approximately separable,allowing the magnetic perturbation to be described as:

$$\delta B(t,\phi) = g(t) f(\phi_R) \text{ with } \phi_R = \phi - \omega t \tag{1}$$

where ϕ_R is the toroidal angle in the system rotating with the perturbation, g is a function describing the overall growth and decay of the perturbation and f is the stiff toroidal mode structure.

In order to investigate the stiff toroidal mode structure again the frame is chosen, in which the perturbation is at rest. After the toroidal shift the profiles are averaged for each toroidal position over time. The criteria for the selection of time instances t to include are:

[1]From the average apparent toroidal velocity a toroidal angle $\phi_{shift}(t)$ is calculated, by which the profile at a given time has to be shifted, to stay in the frame where the main peak is at a fixed toroidal position. To cope with the problem of discretisation of toroidal positions Fourier transformation in combination with the equality $FT(B(\phi+\phi_{shift}(t),t)) = e^{i\phi_{shift}(t)} FT(B(\phi,t))$ is applied. From the obtained Fourier coefficients the shifted profiles in real space are reconstructed.

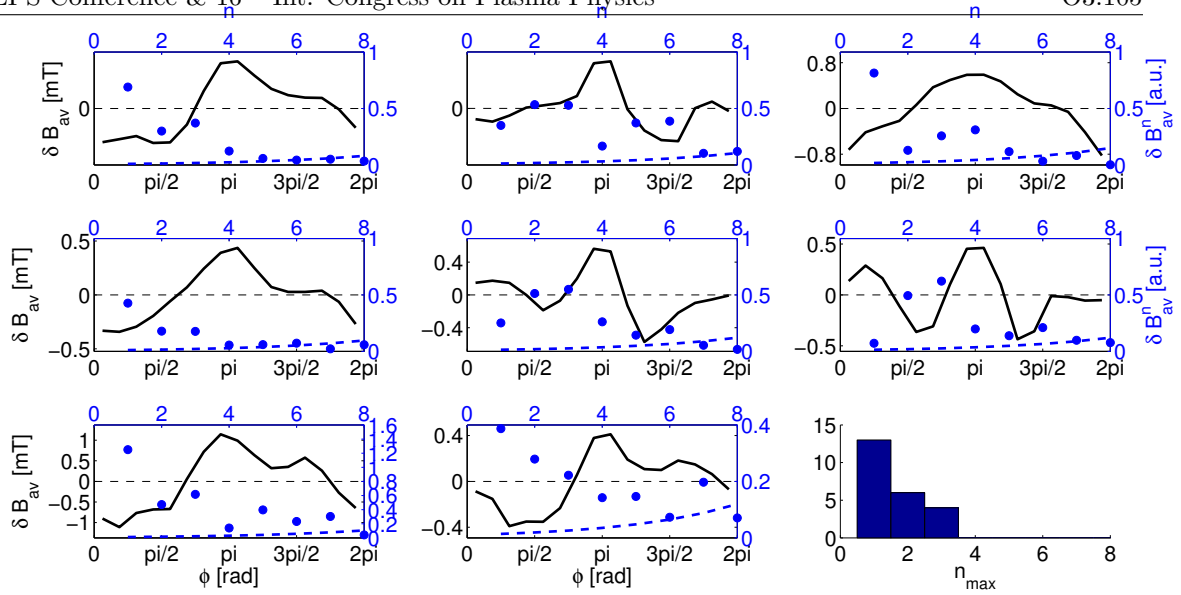

Figure 2: Shifted and averaged toroidal profiles of δB during the growth phase of 8 ELMs in discharge 42062: All figures except the bottom right one show for an individual ELM the magnetic perturbation δB_{av} averaged over a number of selected time instances as a function of ϕ (black). In the same plots the compensated amplitudes of the mode components δB^n_{av} are illustrated (right and top axis, blue). The blue dashed lines represent the Fourier transform of the inter-ELM fluctuation level. The bottom right plot shows the histogram of the mode number n_{max} corresponding to the maximum compensated amplitude of the mode component over a set of 23 ELMs

.

1. $\delta B_{traj}(t) > 0.5 \cdot max(\delta B_{traj})$,
2. the set of time instances is without gaps and ends at $t = t(\delta B_{traj} = max(\delta B_{traj}))$.

Normalization to the overall growth described by g in equation 1 is not applied, as the variation in profile peak (dip) size is limited by the first selection criterion. More than 50% of the ELMs are deselected due to failure of the tracing algorithm or less than 4 time instances fullfilling the criteria. Figure 2 displays the shifted and averaged profiles of δB for 8 ELMs in discharge 42062. A considerable range of profile shapes can be observed. In most cases the entire toroidal circumference is affected by a significant perturbation.

The radial decay of magnetic perturbations depends on the local poloidal mode number, which is determined by the local field line inclination in combination with the toroidal mode number. Close to the separatrix at the LFS the local field line inclination is almost constant. Therefore it is straight forward to compensate this radial decay in the Fourier representation. The extent of the radial decay is estimated by a code evaluating synthetic probe signals evoked by a mode in the plasma edge, which is represented as a superposition of current filaments [9]. An exponential fit gives a radial decay of

$$\delta B / \delta B_{mode} \propto (r/r_P)^{-0.91 \cdot n}, \tag{2}$$

where δB_{mode} is the magnetic perturbation at the mode location (plasma edge), $r/r_P \sim 1.41$ is the ratio of minor radii of probe and mode location and n is the toroidal mode number.
Figure 2 displays in blue amplitudes of the mode components of δB_{av}, where the mode number dependent radial decay is compensated. Higher absolute values of the amplitude of the mode component for low toroidal mode numbers can be observed as a general trend. This is confirmed by the bottom right plot in figure 2, which displays the histogram of the mode number n_{max} corresponding to the maximum compensated amplitude of the mode component for the set of ELMs selected. The $n = 1$ component is the strongest for the majority of these ELMs.
The Fourier transform of the inter-ELM fluctuation level has been indicated as a dashed line in figure 2. Only in some cases the absolute value of the coefficients corresponding to higher toroidal mode numbers are below this level. However this casts no doubt on the general trend of components with low toroidal mode number dominating. Furthermore by comparison of the signs of the toroidal velocities of the main profile peak and the phase of the Fourier coefficients a dominant aliasing effect has been excluded.

In this paper it has been demonstrated that the magnetic perturbations in the ELM growth phase of a relatively strongly heated TCV discharge has a stiff toroidal mode structure. This stiffness is a sign of coupling of toroidal mode components. As this is incompatible with a linear perturbation it indicates non-linear interaction. Furthermore it has been shown that in this phase $n = 1$ is the dominant component of this stiff toroidal mode structure in the majority of cases. This is of special significance when compared to results from linear stability analysis [10]. Here a toroidal mode number n of 1 or 2 is even below mode numbers of the most unstable modes for typical kink/peeling modes ($n \sim 3-6$) and clearly below the ones for typical peeling-ballooning modes ($n \sim 5-20$). In summary there is a strong indication that in contrast to the linear ELM phase in the non-linear ELM phase low toroidal harmonics ($n = 1-2$) become the dominant component of the perturbation.

References

[1] G. Huysmans and A. Loarte. *J.Nucl.Mater., submitted*, (2012).

[2] P. B. Snyder, H. R. Wilson, and X. Q. Xu. *Physics of Plasmas*, **12** (2005).

[3] S. Coda for the TCV team. *Nuclear Fusion*, **51** (2011), 094017.

[4] J. Rossel, J.-M. Moret, et al. *Nuclear Fusion*, **52** (2012), 032004.

[5] J.-M. Moret, F. Buhlmann, et al. *Review of Scientific Instruments*, **69** (1998), 2333.

[6] M. Valovic et al. *21th EPS Conference on Controlled Fusion and Plasma Physics*, (1994).

[7] J. Neuhauser, V. Bobkov, et al. *Nuclear Fusion*, **48** (2008), 045005.

[8] R. Wenninger et al. *Accepted by Nuclear Fusion - preprint available at http://arxiv.org/abs/1202.3603*, (2012).

[9] H. Reimerdes, O. Sauter, et al. *Phys. Rev. Lett.*, **88** (2002), 105005.

[10] P. Snyder, N. Aiba, et al. *Nuclear Fusion*, **49** (2009), 085035.